Determination of drag coefficients in ball bearings and automatic ball balancers at low Reynolds numbers

Lars Spannan[a,*] and Elmar Woschke[a]

[a]Otto von Guericke University, Universitätsplatz 2, 39106 Magdeburg, Germany

ARTICLE HISTORY
Compiled April 9, 2020

ABSTRACT
In rolling element bearings, the influence of drag induced by the lubricant is predominantly considered in the context of efficiency loss estimations, whereas the movement of the rolling elements is mainly constrained by the contact with the bearing rings and, if present, the cage. However, automatic ball balancers, which are installed in rotating machinery to reduce unbalance excitation, are in design very similar to fully lubricated ball bearings missing the cage, the inner ring and the majority of the balls. Inherent to the functional principle, the balancing efficiency and stability are significantly influenced by the choice of lubricant and resulting drag forces. Therefore, the estimation of the drag coefficient based on the geometry and lubrication of automatic ball balancers plays an important role in the engineering process.

With a focus on the Stokes flow regime, the drag coefficient for a single sphere in an annular flow domain is determined numerically with finite volume discretization and the SIMPLE steady state solution scheme. In order to derive an empirical relation between the design of the automatic ball balancer and resulting drag coefficients a parameter study is conducted.

As a result, a drag model based on the balancer geometry and the lubrication fluid properties is presented, which helps to supplement a large number of published kinetic models regarding the analysis of automatic ball balancer stability and transient behaviour.

KEYWORDS
ball bearing; drag; Stokes flow; automatic balancing

Preprint

1. Introduction

The calculation of drag forces resulting from flows around spheres and cylinders are widely used benchmarks to evaluate computational methods in the area of fluid mechanics due to the simplicity of the geometry, see for example Johnson and Patel (1999), Jones and Clarke (2008) and Bayraktar, Mierka, and Turek (2012). When defining a large computational domain compared to the dimensions of the obstacle, the effect of domain boundaries on the solution is attenuated in order to represent the targeted free flow condition. In the study at hand, however, the drag of a sphere confined in an annular domain is examined in the context of automatic balancing of rotating machinery.

The concept of automatic balacing describes the arrangement of balancing masses, usually balls, in relation to the axis of rotation of a rotor in order to compensate its

* CONTACT L. Spannan. Email: lars.spannan@ovgu.de ORCiD: 0000-0003-3237-4405

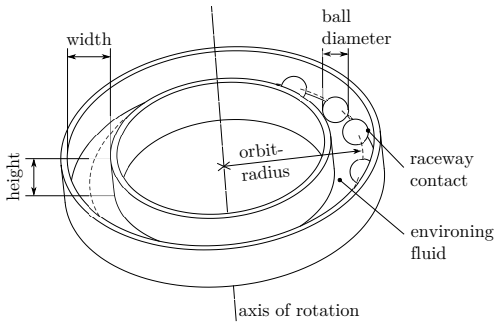

Figure 1. Principle design of automatic ball balancers.

unbalance. Depending on the application, the unbalance can vary during operation, for example laundry in washing machines, samples in laboratory centrifuges or abrasion induced imbalance in angle grinders.

Since the friction between the balls and the rotor cavity in which they are orbiting around the rotor axis has negative influence on the accuracy of the unbalance compensation, the outer rings of ball bearings are often used in the design to decrease friction as presented by Lindell (1996) for the application in angle grinders. Therefore, the basic design of the automatic balancer can be described as a radial ball bearing missing the inner ring, the cage and the majority of the balls, see figure 1. In addition to the balls, the cavity is filled with a viscous fluid, which influences the dynamics and noise emission of the automatic balancing unit. As a result, the movement of the balls in the annulus cavity is significantly affected by drag forces, which are to be determined by numerical analysis in the presented study.

The determination of drag on spheres considering contact with domain boundaries is examined in several research publications. Goldman, Cox, and Brenner (1967), for example, studied the slow motion of a sphere in contact with a plane wall using asymptotic solutions of the Stokes equations. Jan and Chen (1997) conducted experiments with a sphere rolling down an inclined plane and derived an empirical relation between the drag coefficient c_d and the corresponding Reynolds number Re. Miyamura, Iwasaki, and Ishii (1981) derived wall correction factors for spheres in contact with cylinders and parallel plates experimentally. Numerical investigations on drag in rolling element bearings were carried out by Marchesse, Changenet, and Ville (2014) focusing on the tandem effect of multiple spheres in a row.

The simulations presented in the following sections yield the drag coefficient of a single sphere in contact with the geometry of an outer radial ball bearing ring confined in an annular domain. The flow conditions are limited to low Reynolds numbers and therefore lead to a laminar flow regime in which the product of Reynolds number and drag coefficient equals a constant. Section 2 describes the configuration of the simulations carried out with the OpenFOAM[1] software. The resulting drag coefficients for different Reynolds numbers as well as a subsequent parameter study, which analyses the influence of the ball orbit radius, the ball diameter and the cavity dimensions are presented in section 3. With the chosen parameter range, the design space of commercially available regular radial ball bearings is covered. Section 4 specifies how the identification of the reciprocal relationship between the drag coefficient and Reynolds number in laminar flow regimes helps with the parametrisation of a variety of kinetic models of automatic ball balancers published in the literature. A concluding discussion

[1]OpenFOAM7 Version 20190708

Preprint

and outlook is given in section 5.

2. Methods

Since the Stokes flow regime at low Reynolds numbers is considered, a symmetric flow regarding the axial geometric symmetry plane is assumed, see figure 2. The inlet and outlet of the curved domain are defined in a suitable distance to the sphere spanning an orbital angle of 60° so that the assumption of a periodic flow condition can be implemented while reducing the computational effort. An increase of the orbital angle to 90° in the calculation of the reference balancer design, section 3, showed no significant influence on the result, substantiating the proposed approach.

Since the sphere has a single contact point with the raceway of the outer ring, the geometry of the domain is altered by introducing a cylindrical column connecting the sphere and the raceway, see figure 2. The column diameter is set to 16 % relative to the sphere diameter. While the impact on the results is believed to be marginal, this modification improves the meshing and solution process.

In order to reduce the computational effort, the case of a sphere orbiting inside the annular domain with an orbital angular velocity of Ω, an orbit radius of R_{orbit} and a ball radius of r_{ball}, see figure 3, is viewed regarding a coordinate system originating in the center of the sphere with the X-axis pointing outwardly in radial direction and the Y-axis pointing in axial direction. As a result, an invariant mesh can be utilized and under the assumption of ideal rolling of the sphere, i.e. no slip occurs in the contact point, the following boundary conditions are defined on the domain boundaries depicted in figure 2:

- symmetry plane: Symmetry boundary condition justified by the low Reynolds numbers resulting in laminar flow.
- inlet: Normal flow into the domain. The velocity magnitude of each cell face is determined by the product of Ω and the distance to the symmetry axis of the annulus.
- outlet: Zero pressure outlet.
- walls: Constant wall velocity defined by the product of Ω and the distance of the cell face to the symmetry axis of the annulus.
- sphere surface: Fixed velocity boundary condition. The velocity is defined by the product of ω and the distance to the Y-axis going through the sphere center. ω results from the ideal rolling condition $\Omega\,(R_{\mathrm{orbit}} + r_{\mathrm{ball}}) = \omega\, r_{\mathrm{ball}}$.

The OpenFOAM simpleFoam application uses the semi-implicit method for pressure-linked equations (SIMPLE) for a steady-state solution of the continuity equation

$$\nabla \cdot \vec{u} = 0 \tag{1}$$

and the momentum equation

$$\nabla \cdot (\vec{u} \otimes \vec{u}) - \nabla \cdot \sigma = -\nabla p_k + \vec{S}_u, \tag{2}$$

where $\vec{u}$, p_k, σ, $\vec{S}_u$ describe the velocity vector, the kinematic pressure, the stress tensor and the momentum source, respectively. The equations for velocity and kinematic pressure are solved iteratively. As a result, for each mesh element three degrees of freedom for the velocity and one degree of freedom for the pressure are determined.

Preprint

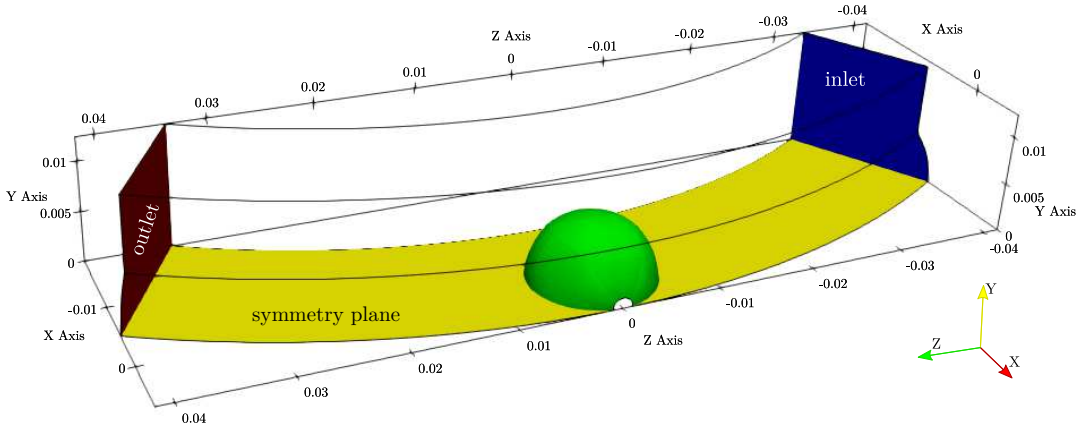

Figure 2. The computational domain. Walls are not shown but indicated by their outlines. The transparent semi-circle at $Z = 0$, $Y = 0$ is resulting from the connecting column avoiding a singular contact point.

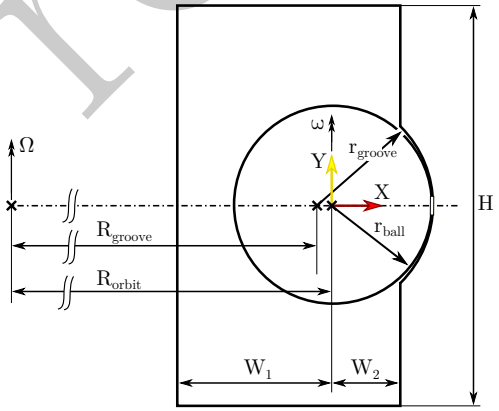

Figure 3. Slice of the domain in the XY-plane ($Z = 0$).

Preprint

Table 1. Number of cells for different mesh refinements.

Mlvl	No. of cells
1	142 000
2	1 136 000
3	3 834 000
4	9 088 000
5	17 750 000

Table 2. Automatic ball balancer reference geometry.

Property	Value
R_{orbit}	77 mm
$r_{\text{ball}}/R_{\text{orbit}}$	0.08
$r_{\text{groove}}/r_{\text{ball}}$	1.2
H/r_{ball}	4.0
W_1/r_{ball}	1.554
W_2/r_{ball}	0.690

In the conducted calculations, the iterations are stopped when the residuals fall below 2×10^{-6}. A structured mesh is generated with the OpenFOAM blockMesh utility and different mesh refinement levels are realized, see table 1. The mesh refinement level (Mlvl) scales the number of cell divisions per block in the computational domain. The mesh is defined for half of the computational domain, see figure 4, and mirrored on the XY-plane.

3. Results

The domain geometry for the study is determined by the properties given in figure 3 and table 2 representing an automatic ball balancer prototype available to the authors. The mesh refinement study in figure 5 shows that the resulting drag coefficient for a Reynolds number $\text{Re} = 1$ does not change significantly between refinement levels four and five, therefore all consecutive simulations are conducted with refinement level four. For different Reynolds numbers in the range of $\text{Re} = 0.01 \ldots 100$ the drag coefficients are determined and are shown in figure 6 along with data from the literature for the free flow condition published by Morrison (2013), the flat surface contact published by Jan and Chen (1997) and experimental results gained for the balancer prototype in the prevalent double logarithmic diagram. In the previous work of Spannan, Daniel, and Woschke (2017) the utilized experimental method, based on the equilibrium evaluation between drag forces and gravitational forces, is presented. In order to derive the drag coefficient c_d for different Reynolds numbers the balancing device prototype is driven on a horizontally aligned axis and the balance of forces is examined. For the considered range of low Reynolds numbers, measurements with silicone oil of kinematic viscosities $\nu_1 = 50\,\text{mm}^2\,\text{s}^{-1}$, $\nu_2 = 298\,\text{mm}^2\,\text{s}^{-1}$ and $\nu_3 = 715\,\text{mm}^2\,\text{s}^{-1}$ are used as reference for the conducted CFD simulations. For a detailed description of the experimental procedures

Preprint

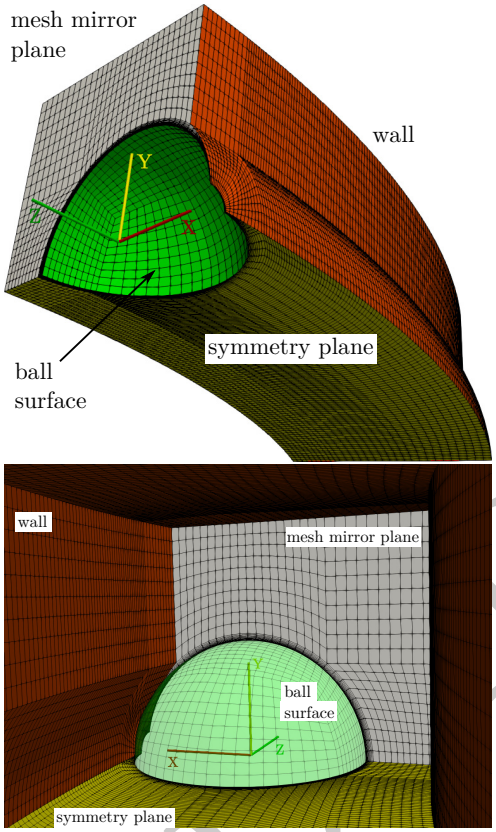

Figure 4. Defined mesh for the coarsest discretization setting (Mlvl = 1) prior to the mirroring operation on the XY-plane. View from the outside (top) and from inside the domain (bottom).

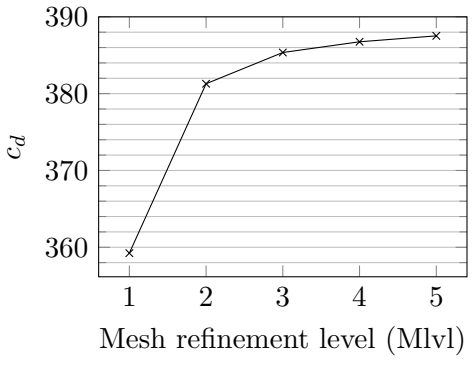

Figure 5. Mesh independence study for the reference configuration of the balancer geometry and a Reynolds number of one.

Preprint

the reader is kindly advised to the given reference.

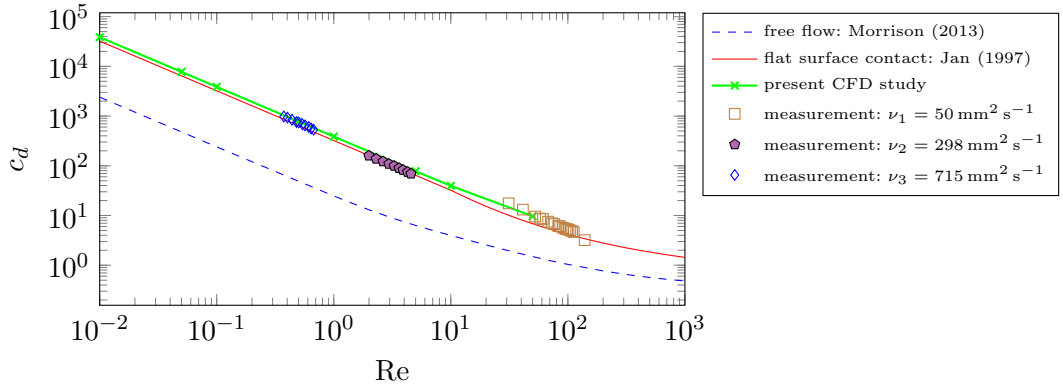

Figure 6. Drag coefficient of flow around a sphere depending on the Reynolds number.

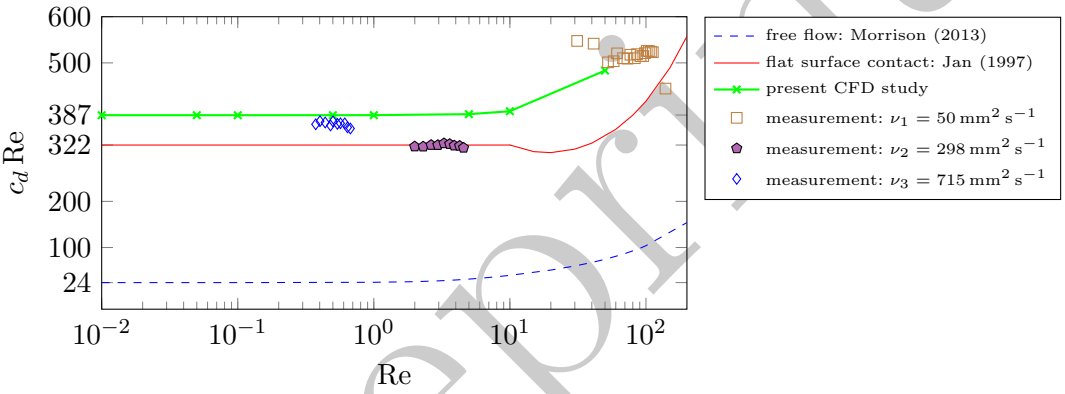

Figure 7. Product of drag coefficient and Reynolds number at low Reynolds numbers.

Figure 6 shows an increased drag coefficient for the considered range of Reynolds numbers compared to the results of the flat surface contact. This result is expected due to the additional confinement of the flow influenced by the domain geometry. Since only the Stokes flow regime is considered, where the product of drag coefficient and Reynolds number result in a constant, the results are transformed to figure 7 showing the product $c_d\,\mathrm{Re}$ for Reynolds numbers up to $\mathrm{Re} = 100$. The simulation results present a constant value of $c_d\,\mathrm{Re} = 387$ and agree well with the experimental data gained for Reynolds numbers $\mathrm{Re} = 0.1 \ldots 0.7$ and the oil with a kinematic viscosity $\nu_3 = 715\,\mathrm{mm^2\,s^{-1}}$. The deviations of the experimental results acquired with the oil of a kinematic viscosity $\nu_2 = 298\,\mathrm{mm^2\,s^{-1}}$ are believed to be caused by friction induced temperature fluctuations during operation and associated viscosity variations. In addition, the agreement between the numerical and the experimental results for Reynolds numbers around $\mathrm{Re} = 100$ is given so that it can be assumed that the solution approach is also applicable for the transition area after the Stokes flow regime. Since the overall agreement is acceptable, the presented simulation model is considered sufficient to gain useful results for a subsequent parameter study.

Preprint

3.1. Parameter study

Although the presented numerical model can supplement the design process of automatic ball balancers by determining drag coefficients for a given geometry at low Reynolds numbers, the possibility of reducing the calculation time and effort by deriving an empirical relation based on a parameter study is investigated in the following. As described previously, the utilization of radial ball bearing components in automatic ball balancers is advantageous due to low friction. With commonly available radial ball bearings in mind, the variance of the drag coefficient for orbitradii in the range $R_{\mathrm{orbit}} = 5\,\mathrm{mm} \ldots 300\,\mathrm{mm}$ and relative ball sizes $r_{\mathrm{ball}}/R_{\mathrm{orbit}} = 0.05 \ldots 0.3$ are considered in the parameter study. The annulus height compared to the ball radius varies only slightly between different bearing sizes and is therefore held constant with $H = 4r_{\mathrm{ball}}$. Similarly, also the groove depth ratio W_2/r_{ball}, see figure 3, is believed to vary only slightly and is held constant. The distance between the ball center and the inner boundary of the fluid domain may vary for different designs of automatic ball balancer units. With regard to compact designs, low values for the clearance W_1/r_{ball} to the inner annulus boundary are to be expected. By increasing the distance, it was checked at what point the influence of the inner boundary becomes negligible.

Based on the evaluation of the dimensionless units Reynolds number and drag coefficient, it is apparent that the change in the orbit radius R_{orbit} has no influence on the result, if the remaining proportion quantities in table 2 remain constant. The check can be carried out quickly by using the converged velocity field of one solution and scale it inversely to the orbit radius magnification. From this initial field solution the convergence is achieved promptly.

Increasing the relative ball radius $r_{\mathrm{ball}}/R_{\mathrm{orbit}}$ results in an increase of the product of Reynolds number and drag coefficient, see figure 8. The calculations are conducted with increasing relative ball size while using the same number of cells.

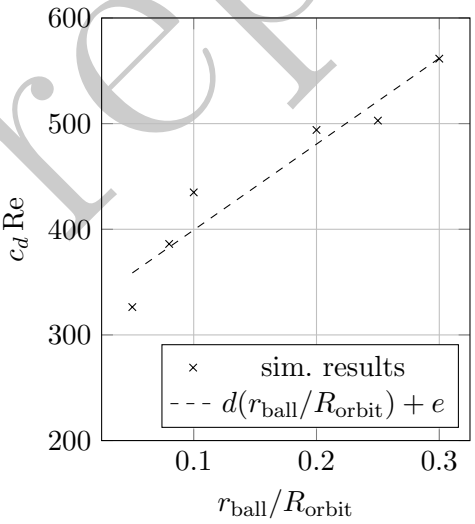

Figure 8. Variation of drag resistance depending on relative ball size. The parameters of the shown linear approximation are $d = 813$, $e = 318$.

The study of increasing distance between the inner boundary of the annular domain and the sphere, figure 9, shows a decay in drag, which can be approximated by an exponential relation with an asymptotic value for large radial clearances. Clearances $W_1/r_{ball} > 2.5$ result in values $c_d\,\mathrm{Re} < 322$, which was identified by Jan and Chen

Preprint

(1997) for the flat surface contact. The decreased drag is attributed to the groove in the outer ring. While increasing the domain volume, the number of cell divisions in radial direction are increased accordingly. Furthermore, the mapFields application of OpenFOAM is utilized to copy a previous solution to the coincident part of the domain. Starting with the solution for $W_1/r_{ball} = 5$ and consecutively decreasing the domain volume, the collective computational effort is reduced.

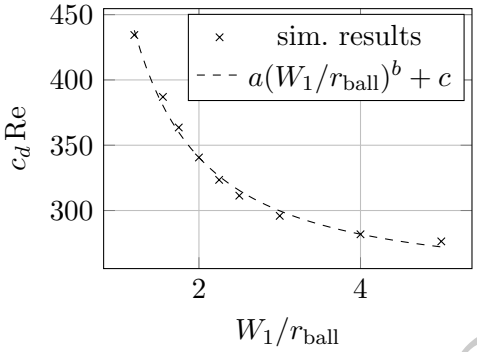

Figure 9. Variation of drag resistance depending on distance to the inner radial boundary. The parameters of the shown exponential approximation are $a = 248$, $b = -1.375$, $c = 245$.

Based on the presented simulation results, neglecting interdependence of the two variables, the relation

$$c_d\,\mathrm{Re} = a\left(\frac{W_1}{r_{\mathrm{ball}}}\right)^b + c + d\left(\frac{r_{\mathrm{ball}}}{R_{\mathrm{orbit}}} - 0.08\right), \tag{3}$$

with $a = 248$, $b = -1.375$, $c = 245$ and $d = 813$, is proposed in order to approximate the resulting drag in the Stokes regime of a single ball in an automatic ball balancer. Since equation (3) emerges from the parameter study based on the reference geometry given in table 2 the best agreement is expected near $W_1/r_{\mathrm{ball}} = 1.554$ and $r_{\mathrm{ball}}/R_{\mathrm{orbit}} = 0.08$.

4. Application

One of the most researched kinetic models for the application of automatic ball balancers is that of a planar oscillator, figure 10, with x, y, φ_{rotor}, φ_{ball} being the two translatoric degrees of freedom, the rotation of the rotor and the orbital position of the ball, respectively. In the derivation of the equations of motion the viscous damping forces due to the fluid inside the cavity is commonly modeled in a linear manner, e.g. a drag moment

$$M_{\mathrm{Drag}} = \beta(\dot{\varphi}_{\mathrm{rotor}} - \dot{\varphi}_{\mathrm{ball}}), \tag{4}$$

proportional to the difference of the rotor angular velocity and the ball orbit velocity, is introduced. See for example Sharp (1975) and Sperling, Ryzhik, and Duckstein (2004).

In several works the importance of the viscous forces is recognised and simulations are conducted in order to identify values for the coefficient β, which lead to optimal

Preprint

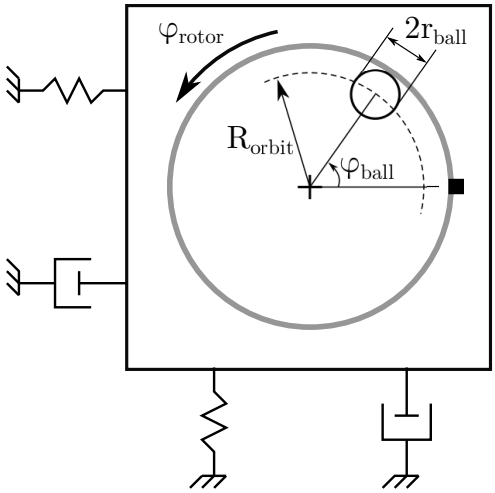

Figure 10. Example of a planar oscillator with an automatic ball balancer.

dynamic behaviour of the rotor system. See for example Ryzhik, Sperling, and Duckstein (2003) for the analysis of rotor run ups and Bykov and Kovachev (2018) for the identification of stable operating speeds of automatic balancing devices. However, concrete correlations between the introduced constant viscous coefficient, β in equation (4), and the design of the balancing unit as well as fluid density and viscosity are not discussed.

Considering the familiar equation for drag forces, the discussed drag moment can be written in the form

$$\begin{aligned} M_{\text{Drag}} &= F_{\text{Drag}}\, R_{\text{orbit}} \\ &= \frac{1}{2}\rho\, A_{\text{ref}}\, c_d\, v_{\text{ref}}^2\, R_{\text{orbit}}\, \text{sign}(v_{\text{ref}}) \\ &= c_d\, \text{Re}\, \frac{\pi}{4}\rho\, \nu\, r_{\text{ball}}\, R_{\text{orbit}}^2\, \dot{\varphi}_{\text{ref}}\,, \end{aligned} \tag{5}$$

with ρ, ν, A_{ref}, v_{ref} being the fluid density, the fluid kinematic viscosity, the cross-sectional area of the ball and the reference flow velocity, respectively. The Reynolds number is introduced as

$$\text{Re} = \frac{2\, r_{\text{ball}}\, v_{\text{ref}}}{\nu}. \tag{6}$$

Under the assumption that $v_{\text{ref}} = \Omega R_{\text{orbit}}$ and $\dot{\varphi}_{\text{ref}} \approx \dot{\varphi}_{\text{rotor}} - \dot{\varphi}_{\text{ball}}$, meaning that the fluid is rotating with the rotor angular velocity, the coefficient β can be identified as a constant

$$\beta = c_d\, \text{Re}\, \frac{\pi}{4}\rho\, \nu\, r_{\text{ball}}\, R_{\text{orbit}}^2. \tag{7}$$

For run up processes of machinery equipped with automatic ball balancing devices the assumption of low Reynolds numbers does not hold generally and velocity differences between the rotor and the fluid occur. But when steady state operations of automatic ball balancers are considered, the stated assumptions are met. As a result, stability analyses, which incorporate equation (4), see for example Bykov and Ko-

Preprint

vachev (2018), can be conducted solely based on geometric properties of the balancer, fluid properties and the presented identification of the product of the drag coefficient and Reynolds number, see equation (3).

5. Discussion

In the presented study a finite volume approximation solution for the laminar flow around a sphere in an annular domain is presented. The domain geometry is derived from an automatic ball balancer prototype and a parameter study is conducted covering the dimensions of common radial ball bearings. The drag simulation results, in terms of the product of Reynolds number and drag coefficient for a reference geometry, show the anticipated constant numerical value for Reynolds numbers below ten. The increase in drag compared to the case of a sphere in contact with a flat wall discussed in the literature shows the influence of the side walls and the curvature of the domain. It is shown that the knowledge of the product of Reynolds number and drag coefficient is beneficial for the parametrisation of kinetic models for automatic ball balancers. Due to the dependence of the results on the fluid viscosity the calculation of drag forces in automatic ball balancer models is subject to uncertainties in determining the viscosity of the fluid and possible temperature sensitivity.

In contrast to applications of automatic ball balancers utilizing larger numbers of balancing balls in order to increase the maximum compensable imbalance of the rotor, the presented flow simulations consider only one ball neglecting possible tandem effects. Two balls in tandem arrangement on the orbit will reduce the drag forces on the downstream body (Marchesse et al. (2014)) making it worth considering appropriate correction factors to equation (3).

During run-up of rotors equipped with automatic ball balancers the angular acceleration may be sufficient to leave the Stokes flow regime. As a result, the product of Reynolds number and drag coefficient deviates from a constant value. With regard to computational flow simulations, the assumptions of symmetry and laminar flow will not be met, leading to increased effort to gain results for larger Reynolds numbers.

In addition to the viscous forces, the friction forces and possible geometrical deviations of the raceway are influencing the dynamical behaviour of the automatic ball balancing system, see Chao, Sung, and Leu (2005), Green, Champneys, and Friswell (2006) and Bykov and Kovachev (2019) for example. Therefore, a fully coupled fluid structure interaction of automatic balancers, i.e. in multi body simulation models, should only be pursued if the modeling quality of friction and imprecise geometry is also enhanced. Compared to the increased effort resulting from a fully coupled simulation the presented method based on the widely utilized gas-particle flow approach (Henderson (1976)) represents a good compromise, from the authors' perspective.

Acknowledgements

The support of Mr. S. Engel, University of Magdeburg (ISUT), in conducting the fluid viscosity measurements and Mr. S. Koch (IFME) in experimental realisation is greatly appreciated.

Preprint

Notes

The OpenFOAM case files as well as the results presented in the figures of this publication will be accessible in the supplemental material Spannan (2020).

References

Bayraktar, E., Mierka, O., & Turek, S. (2012). Benchmark computations of 3D laminar flow around a cylinder with CFX, OpenFOAM and FeatFlow. *International Journal of Computational Science and Engineering*, *7*(3), 253. https://doi.org/10/ggfp2z

Bykov, V. G., & Kovachev, A. S. (2018). Autobalancing of a rigid rotor in viscoelastic orthotropic supports considering eccentricity of the automatic ball balancer. *AIP Conference Proceedings*, *1959*(1), 080011. https://doi.org/10/gf3s79

Bykov, V. G., & Kovachev, A. S. (2019). Dynamics of a statically unbalanced rotor with an elliptic automatic ball balancer. *Vestnik of Saint Petersburg University. Mathematics. Mechanics. Astronomy*, *6*(64), 452-462. (In Russian) https://doi.org/10/drbz

Chao, P. C.-P., Sung, C.-K., & Leu, H.-C. (2005). Effects of rolling friction of the balancing balls on the automatic ball balancer for optical disk drives. *Journal of Tribology*, *127*(4), 845. https://doi.org/10/cz4tk3

Goldman, A. J., Cox, R. G., & Brenner, H. (1967). Slow viscous motion of a sphere parallel to a plane wall — I motion through a quiescent fluid. *Chemical engineering science*, *22*(4), 637–651. https://doi.org/10/d59wm5

Green, K., Champneys, A., & Friswell, M. (2006). Analysis of the transient response of an automatic dynamic balancer for eccentric rotors. *International Journal of Mechanical Sciences*, *48*(3), 274–293. https://doi.org/10/bgff3w

Henderson, C. B. (1976). Drag coefficients of spheres in continuum and rarefied flows. *AIAA Journal*, *14*(6), 707–708. https://doi.org/10/d52s7q

Jan, C.-D., & Chen, J.-C. (1997). Movements of a sphere rolling down an inclined plane. *Journal of Hydraulic Research*, *35*(5), 689–706. https://doi.org/10/bp4x9v

Johnson, T. A., & Patel, V. C. (1999). Flow past a sphere up to a reynolds number of 300. *Journal of Fluid Mechanics*, *378*, 19–70. https://doi.org/10/b7m2tf

Jones, D. A., & Clarke, D. B. (2008). *Simulation of the flow past a sphere using the fluent code* (Tech. Rep.). Australian Government, Department of Defence. Retrieved from `https://apps.dtic.mil/docs/citations/ADA494935`

Lindell, H. (1996). Vibration reduction on hand-held grinders by automatic balancing. *Central European journal of public health*, *4*(1), 43–45. (PMID: 8996669)

Marchesse, Y., Changenet, C., & Ville, F. (2014). Numerical investigations on drag coefficient of balls in rolling element bearing. *Tribology Transactions*, *57*(5), 778–785. https://doi.org/10/ggfqw4

Miyamura, A., Iwasaki, S., & Ishii, T. (1981). Experimental wall correction factors of single solid spheres in triangular and square cylinders, and parallel plates. *International Journal of Multiphase Flow*, *7*(1), 41–46. https://doi.org/10/d3zd43

Morrison, F. A. (2013). *An introduction to fluid mechanics*. Cambridge University Press. https://doi.org/10/ggfqw5

Ryzhik, B., Sperling, L., & Duckstein, H. (2003). The influence of damping on the efficiency of autobalancing devices for rigid rotors. In *Proceedings of the second international symposium on stability control of rotating machinery ISCORMA-2003* (pp. 104–113). Gdańsk, Poland.

Sharp, R. (1975). An analysis of a self-balancing system for rigid rotors. *Journal of Mechanical Engineering Science*, *17*(4), 186–189. https://doi.org/10/bzcp8d

Spannan, L. (2020). *OpenFOAM case files for drag coefficient determination in automatic ball balancers*. https://doi.org/10.5281/zenodo.xyz

Spannan, L., Daniel, C., & Woschke, E. (2017). Experimental study on the velocity dependent

Preprint

drag coefficient and friction in an automatic ball balancer. *Technische Mechanik*, *37*(1), 62–68. https://doi.org/10/gf3s8h

Sperling, L., Ryzhik, B., & Duckstein, H. (2004). Single-plane auto-balancing of rigid rotors. *Technische Mechanik*, *24*(1), 1–24.

Preprint